Initial Development of a Program for Drone Micro-Doppler Signature Modelling

Jovan Radivojević, Predrag Petrović, Aleksandar Lebl, Mladen Mileusnić

***Abstract*—Micro-Doppler signature spectrograms obtained by FMCW radars are powerful method for malicious drones detection, identification, localization and classification. Our aim in this investigation has been to replace the base of spectrograms recorded on polygons using high number of available drone types by the spectrograms obtained by the application of originally developed program. Initial program development and verification are described in the paper. It is presented how the calculated spectrograms may be used to determine the important parameters of drones' flight and construction: number of blades in a rotor, rotors' angular rotation rate and blades' length which is the first step in a decision about an applied drone type. The presented results are the starting report on our important development devoted to the improvement of overall public safety.**

***Index Terms*—Malicious drone identification; micro-Doppler signature spectrograms; drone hovering; program for drone spectrograms modelling.**

I. Introduction

DRONES or unmanned aerial vehicles (UAVs) implementation brings great benefits in everyday life by replacing human activities in many areas. Drones may perform some important actions more precisely, more promptly than humans and without people risk exposure. But, on contrary, drones may often be the cause of sudden and unexpected danger for human lives and/or the whole world economy [1], [2].

There are solutions based on several sensor types which may be applied to malicious drones' detection, identification, localization and classification (DILC). The most often applied sensors are radars, cameras (optical and infra-red), audio and radio-frequency (RF) sensors. The benefits and drawbacks of each sensor type application are emphasized in [3], [4]. The applied solutions are usually based on several (even three or four) different sensor types [5], [6]. Among the sensors, radar is especially important due to its relative independence or very low dependence on weather and lighting conditions as fog, rain, smoke or darkness [7]. The present solutions are based on two radar types implementation: Frequency Modulated Constant Wave (FMCW radar whose principles of operation are explained in [8]) and Forward Scatter Radar (FSR whose principles of operation are explained in [9]). Drone spectrograms which are obtained by FMCW and FSR radars are especially important for applied drones identification and classification. They are analyzed in a significant number of existing solutions and [10], [11] are just two examples. In the case of FMCW radar, the obtained spectrograms follow from the Doppler effect of drone parts micro motion to the transmitted radar signal. We speak about drones micro-Doppler signatures, i.e. the obtained graphs are specific for each type of drones [12]. In practical situations the special problem is to distinguish drones from other flying objects with similar dimensions (e.g. birds) whose spectrograms may be similar to drone spectrograms [13].

Drones DILC using spectrograms supposes collecting a great number of practical records on the significant number of different drone types. The records have to be made when drones are at different heights, at different distance from radar (meaning at different elevation angles), when they are hovering or when they are flying, when there are more drones present in the same time (drone swarms) and so on. Besides, the spectrograms appearance depends on some specific drones characteristics as the number of drone's rotors, number of blades on each rotor, the length of blades and the rotors' rotation rate (in rounds per minute – RPM or in rounds per second – RPS). So, it is necessary to have different drone types and to make many spectrograms for each type under different conditions. Due to these problems it is important to develop the program which allows spectrograms calculation and presentation (without practical scenarios recording), especially in the initial phases when DILC criteria have to be defined [7], [11], [14].

IRITEL has a great experience in the development, modernization and implementation of radar systems, development of software for radar systems receivers and simulators of radar operation. The contribution [15] has two-fold relation to the solution presented in this paper: as a realized simulator and as it considers radars with Doppler Effect. Micro-Doppler signatures are formed on the base of the received radar signal and IRITEL has developed both simulators of radar signal receivers [16], [17] and practical solutions of these receivers [18], [19]. The control of radar receivers is the subject of contributions [20], [21]. A good-quality generated signal is also important for FMCW radar operation and IRITEL's solutions in this area have an international verification [22], [23]. IRITEL's complete radar systems in the area of AESA radars [24], [25] and in the area of existing radars modernization [26] - [28] are additional guarantee for future successful practical implementation of solution from this paper.

The main theoretical aspects of FMCW radar operation are explained in the Section II. This explanation includes the method how spectrograms are calculated. The block-scheme of the developed program for spectrograms calculation is

Jovan Radivojević is with IRITEL a.d., Batajnički put 23, 11080 Belgrade, Serbia (e-mail: jovan.radivojevic@iritel.com).

Predrag Petrović is with IRITEL a.d., Batajnički put 23, 11080 Belgrade, Serbia (e-mail: presa@iritel.com).

Aleksandar Lebl is with IRITEL a.d., Batajnički put 23, 11080 Belgrade, Serbia (e-mail: lebl@iritel.com).

Mladen Mileusnić is with IRITEL a.d., Batajnički put 23, 11080 Belgrade, Serbia (e-mail: mladenmi@iritel.com).

 ISBN 978-86-7466-930-3

presented in the Section III. Several calculated spectrograms are presented in the Section IV. The suggested method to determine characteristic parameters of drone flight and drone construction is described in the Section V. At the end, the conclusions are in the Section VI.

II. SPECTROGRAM SIGNAL CALCULATION

The signal generated in FMCW radar is sinusoidal and its frequency is linearly variable as a function of time. The drone spectrograms are obtained on the base of the returned echo signal from the moving rotor blades. The echo signal from all blades forming one rotor may be expressed by [29]:

$$S_{\Sigma}(t) = \sum_{k=0}^{N_b-1} s_{lk}(t) = \\ = L \cdot \exp\left(-j\frac{4\cdot\pi}{\lambda}\cdot\left(R_0 + z_0\cdot\sin\beta\right)\right)\cdot \\ \cdot\sum_{k=0}^{N_b-1}\sin c\left(\Phi_k(t)\right)\cdot\exp\left(-j\cdot\Phi_k(t)\right) \tag{1}$$

where it is $\mathrm{sinc}(\Phi_k(t)) = \sin(\Phi_k(t))/(\Phi_k(t))$ and

$$\Phi_k(t) = \frac{4\cdot\pi}{\lambda}\cdot\frac{L}{2}\cdot\cos\beta\cdot \\ \cdot\cos\left(\Omega\cdot t + \varphi_0 + \frac{2\cdot\pi\cdot k}{N_b}\right)\quad (k=0,1,2,...N_b\text{-}1). \tag{2}$$

The sign may be + or – before $\Omega\cdot t$, depending on the direction of the rotor rotation for each unique rotor.

The meaning of variables in these two equations may be expressed with the reference to the Fig. 1:

- L – the length of each blade;
- N_b – number of blades in each rotor (two possibilities are presented separately: rotors with two or three blades);
- R_0 - distance between the radar and the drone rotor (approximately the same as between radar and drone);
- z_0 – drone height;
- β – drone elevation angle;
- Ω – rotor angular rotation rate;
- λ – radar signal wavelength;
- φ_0 – rotor starting rotation angle.

The returned signal from all drone rotors is:

$$S_{\Sigma}(t) = \sum_{i=1}^{N_r}\sum_{k=0}^{N_b-1} s_{lk}(t) = \\ = \sum_{i=1}^{N_r} L\cdot\exp\left(-j\frac{4\cdot\pi}{\lambda}\cdot\left(R_{0i} + z_{0i}\cdot\sin\beta_i\right)\right)\cdot \\ \cdot\sum_{k=0}^{N_b-1}\sin c\left(\Phi_{ik}(t)\right)\cdot\exp\left(-j\cdot\Phi_{ik}(t)\right) \tag{3}$$

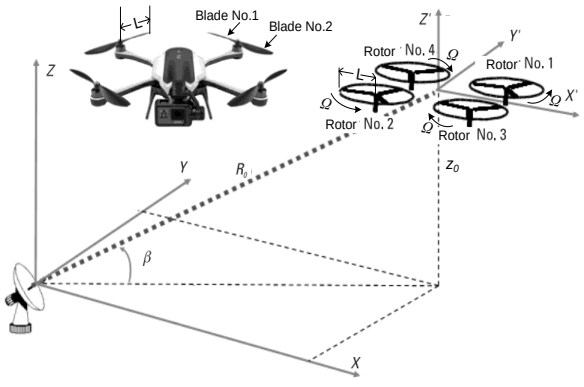

Fig. 1. Parameters included in drone spectrograms calculation

where it is:

$$\Phi_{ik}(t) = \frac{4\cdot\pi}{\lambda}\cdot\frac{L}{2}\cdot\cos\beta_i\cdot \\ \cdot\cos\left(\Omega_i\cdot t + \varphi_{0i} + \frac{2\cdot\pi\cdot k}{N_b}\right)\quad (k=0,1,2,...N_b\text{-}1) \tag{4}$$

and

- N_r - the number of rotors on the drone.

In general case, all rotors have their own specific angular rotation rate Ω_i. The difference in rates may be even more than 2:1 when drone is flying left or right [30]. In our analysis in this paper we consider that drone is hovering. Thus we suppose that all rotors have the same Ω_i. The range of Ω_i values may be estimated on the base of graphs from [31] which present drone performances when rotors angular rotation rate changes in the range 1400-8600 RPM, or, approximately, 20-150 RPS. The direction of rotors rotation is standardized to allow stable flight. In the case of drone with four rotors (quadcopter) two opposite rotors rotate in the clockwise direction and to other opposite rotors rotate in counter clockwise direction [32]. The length of blades when quadcopters or hexacopters are applied varies in the range between 11.9cm and 38.1cm according to some available literature [11], [13], [33]-[36]. The heights z_{0i} for all rotors are also the same as we may assume that drone is always positioned parallel to the ground. The assumption of all R_{0i} values equality is not quite valid. It would be necessary to precisely involve distances between rotor centres to determine exact values of R_{0i}. Nevertheless, we shall also suppose that there is no difference between R_{0i}s without important loss of generality. The elevation angles β_{0i} for all rotors are also practically the same and they are calculated as the ratio of z_{0i} and R_{0i}. Our investigation has been performed for FMCW radar operating at 24GHz, i.e. λ=12.5mm. The most often applied drones have not more than four rotors (quadcopters), but still exist drones with six (hexacopter) or eight (octocopter) rotors [37].

The standard procedure to calculate spectrogram includes calculation of Short Time Fourier Transform (*STFT*) of the considered signal according to the equation [38]:

$$STFT\left(S_n(m,\omega)\right) = \sum_{n=-\infty}^{\infty} S_n\cdot w_{n-m}\cdot\exp\left(-j\cdot\omega\cdot t_n\right) \tag{5}$$

where w_n is the Hanning window defined by [39]:

$$w_n = \frac{1}{2}\cdot\left(1-\cos\frac{2\cdot\pi\cdot n}{N}\right)\quad (n=0,1,2...N) \tag{6}$$

III. PROGRAM STRUCTURE SHORT PRESENTATION

The block-diagram of the program for spectrogram calculation is presented in the Fig. 2.

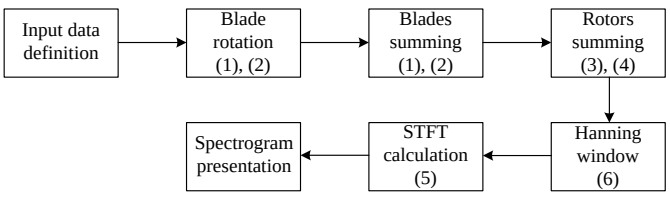

Fig. 2. Block-diagram of the program for spectrogram calculation

The first step in the program flow is to define input data: parameters of drone position towards radar, drone construction and operation, radar signal characteristics and the characteristics of desired spectrogram presentation. The parameters of drone position are its elevation angle (β), its

 ISBN 978-86-7466-930-3

height over ground (z_0) and distance between radar and drone (R_0). The drone construction parameters are the number of drone rotors (N_r), number of blades in each rotor (N_b) and the length of blades (L). Drone operation parameter is its rotors' angular rate (Ω) and direction of rotors rotation (clockwise or counter clockwise). Radar operational frequency (f_r) is the characteristic of radar signal. The characteristic parameters for spectrogram calculation and presentation are time step for spectrogram calculation (t_{step}) and time step for spectrogram display (t_{disp}).

The first step in calculation realization is related to each blade rotation. The calculation procedure follows the equations (1) and (2) in this step. The following step is to sum the echo signals from all single blades forming one rotor. This summing is also the part of equations (1) and (2). The third step in calculation process is to sum all echo signals from drone rotors, according to equation (3) and (4). The final step is related to spectrogram calculation using *STFT* according to the equation (5). Before *STFT* calculation, echo signal is modelled applying Hanning window signal according to the equation (6).

The output result of our calculation is the spectrogram presentation. A new spectrogram is obtained for each selected combination of input data parameters according to their defined values from ranges specified in the previous Section II. This is our initial investigation and this program version is realized in Excel. Some of input parameters could not be selected in the whole specified range according to the data from the Section II. There are three such parameters: the number of rotors is limited to 4 (thus covering the great majority of applied drones), the blade length is limited to 25.4cm (the most drones do not have longer blades according to the presented examples from literature) and the rotor angular rate is limited to about 40 RPS (its usual value is in the range 30-40 RPS [11], [40]).

IV. The Results of Calculation

Figures 3-12 present micro-Doppler signature graphs obtained by the implementation of our program. In all these cases it is considered that a drone has four rotors (N_r=4) and that it is positioned at a distance R_0=100m. The parameters which are varied are: 1) the number of blades constituting each rotor (N_b=3 in the figures 4, 5, 6, 7 and 9, N_b=2 in the remaining figures); 2) the length of blades (L=0.12m in the Fig. 5, L=0.18m in the Fig. 6, L=0.24m in remaining figures); 3) rotor angular rotation rate (Ω=20RPS in the figures 9 and 10, Ω=40RPS in the figures 7 and 8, Ω=30RPS in the remaining figures) and 4) the elevation angle i.e. the drone height over the ground (z_0=77m in the Fig. 11, z_0=94.8m in the Fig. 12, z_0=30m in the remaining figures). The frequency division 0-200Hz on the vertical axis of spectrograms is not the absolute value of Doppler shift for the applied 24GHz radar. It is a consequence of frequency bandwidth compression when STFT is calculated and it approximately corresponds to the compression factor 20.

The legends on the right side of figures 3-12 present the signal level (in dB) at the corresponding figure. The frequency components with the higher level in the range between -20dB and +10dB (which are presented in the brown, red and orange colour) are important for the spectrogram analysis. The other components are of lower or significantly lower level and are not important for consideration. The transition between the part of the graph with the higher frequencies level and the part of the frequencies with the low signal level (lower than -40dB which is presented by turquoise, blue and pink colour) is on all graphs rather sharp. The bandwidth of the area in brown, red and orange colour depends on the value of some parameters for which the graphs are calculated.

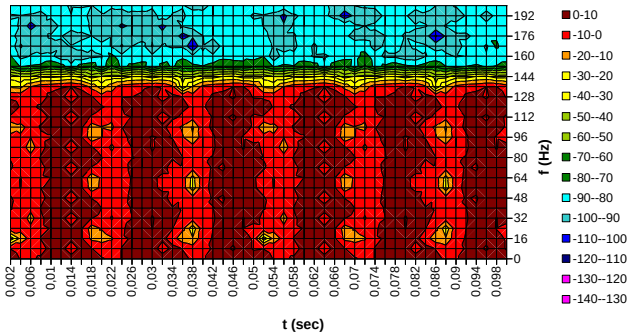

Fig. 3. Micro-Doppler signature of a drone with N_r=4, N_b=2, L=0.24m, R_0=100m, z_0=30m, Ω=30RPS

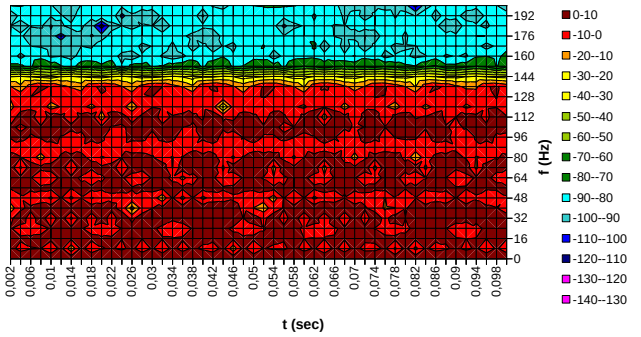

Fig. 4. Micro-Doppler signature of a drone with N_r=4, N_b=3, L=0.24m, R_0=100m, z_0=30m, Ω=30RPS

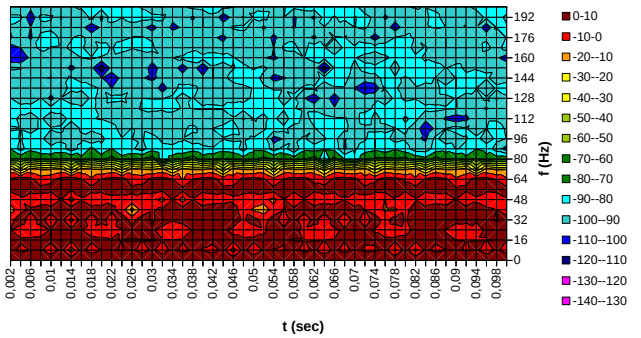

Fig. 5. Micro-Doppler signature of a drone with N_r=4, N_b=3, L=0.12m, R_0=100m, z_0=30m, Ω=30RPS

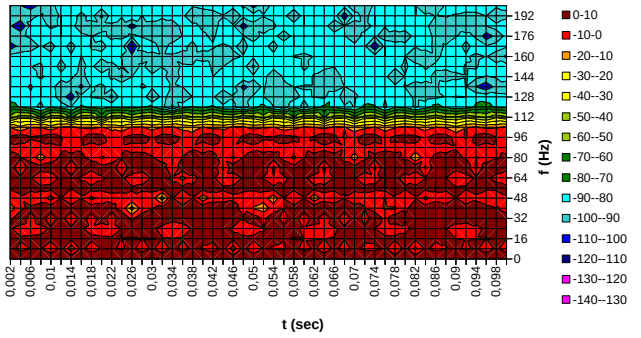

Fig. 6. Micro-Doppler signature of a drone with N_r=4, N_b=3, L=0.18m, R_0=100m, z_0=30m, Ω=30RPS

 ISBN 978-86-7466-930-3

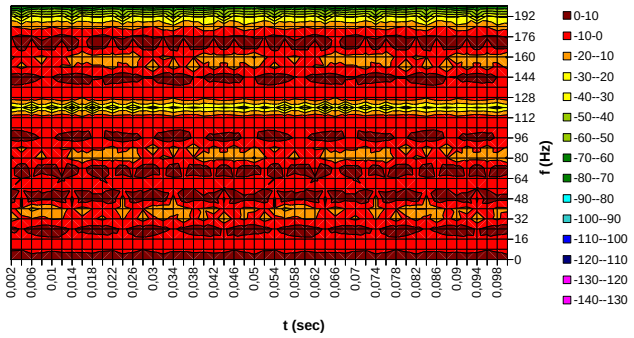

Fig. 7. Micro-Doppler signature of a drone with N_r=4, N_b=3, L=0.24m, R_0=100m, z_0=30m, Ω=40RPS

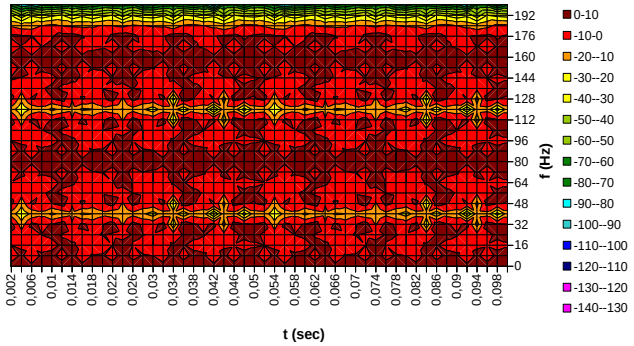

Fig. 8. Micro-Doppler signature of a drone with N_r=4, N_b=2, L=0.24m, R_0=100m, z_0=30m, Ω=40RPS

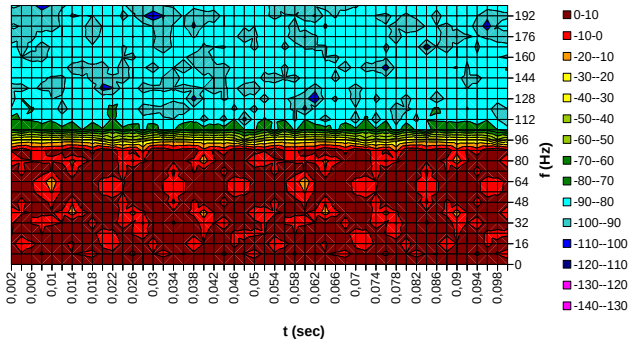

Fig. 9. Micro-Doppler signature of a drone with N_r=4, N_b=3, L=0.24m, R_0=100m, z_0=30m, Ω=20RPS

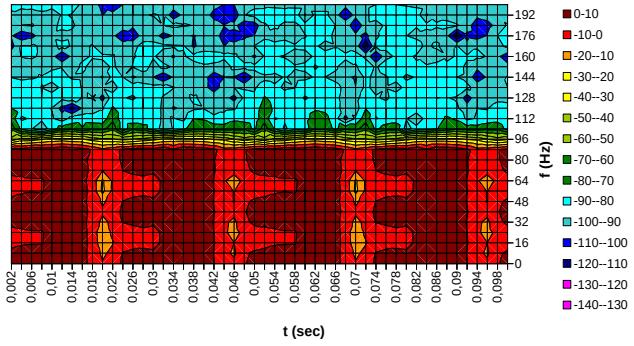

Fig. 10. Micro-Doppler signature of a drone with N_r=4, N_b=2, L=0.24m, R_0=100m, z_0=30m, Ω=20RPS

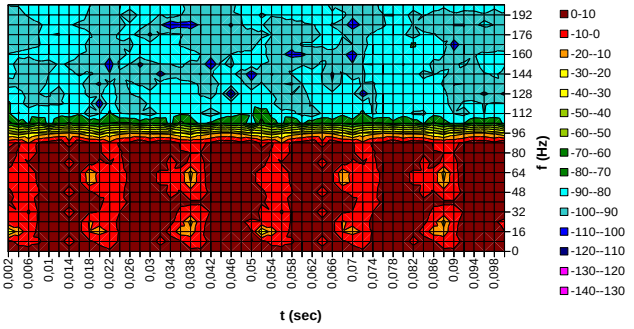

Fig. 11. Micro-Doppler signature of a drone with N_r=4, N_b=2, L=0.24m, R_0=100m, z_0=77m, Ω=30RPS

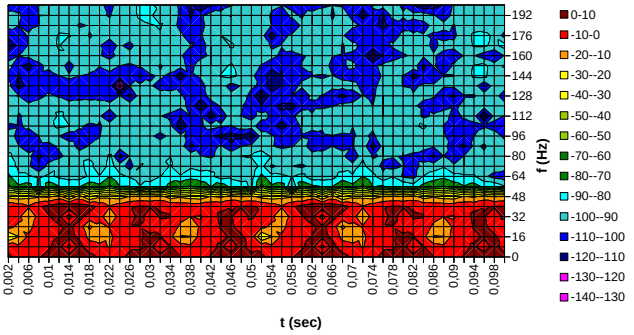

Fig. 12. Micro-Doppler signature of a drone with N_r=4, N_b=2, L=0.24m, R_0=100m, z_0=94.8m, Ω=30RPS

The number of blades in each rotor does not have any influence on the frequency bandwidth of the area with higher signal level. This is approved mutually comparing Fig. 3 (N_b=2, Ω=30RPS) and Fig. 4 (N_b=3, Ω=30RPS), then Fig. 7 (N_b=3, Ω=40RPS) and Fig. 8 (N_b=2, Ω=40RPS) and, finaly, Fig. 9 (N_b=3, Ω=20RPS) and Fig. 10 (N_b=2, Ω=20RPS). When comparing these cases two by two, we see that the number of blades only causes different configuration of brown, red and orange surfaces within the area of higher signal level.

The blades' length has the influence on the frequency bandwidth of the area with higher signal level. Dependence may be considered as linear according to the mutual comparison of the figures 4, 5 and 6. The width is approximately Δ=70Hz when it is L=0.12m (Fig. 5), Δ=104Hz when it is L=0.18m (Fig. 6) and Δ=140Hz when it is L=0.24m (Fig. 4).

The rotor angular rotation rate also has the influence on the frequency bandwidth of the area with higher signal level. Dependence is also linear, as in a case of blades' length. This statement is approved considering the graphs in the figures 9 and 10 (the width is Δ=94Hz at Ω=20RPS), then figures 3 and 4 (the width is Δ=140Hz at Ω=30RPS) and figures 7 and 8 (the width is Δ=186Hz at Ω=40RPS).

The frequency bandwidth of the area with higher signal level is proportional to the cosine value of the elevation angle. This is obvious comparing the graphs in the figures 3, 11 and 12. The drone heights (z_0=30m, z_0=77m and z_0=94.8m) are selected in such way that the ratios $\cos(z_0/R_0)$ in these three cases are 0.954, 0.638 and 0.318 or proportional to 3:2:1. The corresponding widths of the area with higher signal level in the figures 3, 11 and 12 are Δ=140Hz, Δ=96Hz and Δ=48Hz respectively, which is very near to 3:2:1.

 ISBN 978-86-7466-930-3

It is possible to distinguish graphs for the drones which have rotors with two blades (figures 3, 8, 10, 11 and 12) from those which have three blades (the remaining five figures). The characteristics when there are 2 blades usually have clearly separated, periodic parts with the highest signal level between 0dB and +10dB (brown segments). The shape of these parts depends on the rotation starting angle. There are six such parts in the figures 3, 11 and 12, eight in the Fig. 8 and four in the Fig. 10. It means that the number of repeatable parts (N_p) when there are 2 blades may be expressed as

$$N_p = N_r \cdot \Omega \cdot T_p \tag{7}$$

where T_p is the time interval of spectrogram investigation.

When there are 3 blades such clear periodic parts may not be easily islolated.

V. Reading the Parameters of Drone Flight and Construction from Spectrograms

In the Section IV it is investigated how the parameters of drone flight and of the drone construction affect its micro-Doppler signature appearance. Frequency bandwidth of the area with higher signal level depends on 3 parameters: blades' length, rotors' angular rotation rate and drone elevation angle. The spectrogram itself gives two values for the calculation. The first one is the frequency bandwidth of the area with higher signal level and the second one is the number of periodic areas with the highest signal level. So, it is necessary to determine one of the three parameters in some other way, not from spectrogram. The most logical is that this parameter is elevation angle β because it may be also determined by some algorithm implementation on FMCW radar [41], [42] (the concrete algorithm for this function is not studied in this paper).

In order to determine L and Ω from some measured spectrogram let us start from the spectrogram from the Fig. 13, which is calculated for the same parameters as in the Fig. 3 with only the exception that it is z_0=0m, i.e. cos(β)=1. It follows from the graph in the Fig. 13 that it is now Δ=148Hz. In this paper we have concluded that this value of Δ is proportinal to Ω and L. This statement may be expressed mathematically as

$$K_m \cdot L \cdot \Omega = 148 \tag{8}$$

Our goal is to determine the value of multiplication coefficient K_m.

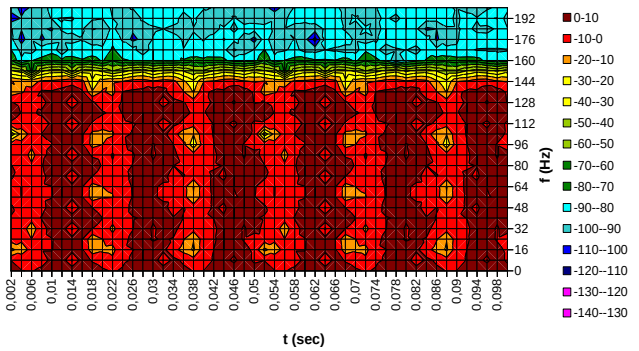

Fig. 13. Micro-Doppler signature of a drone with N_r=4, N_b=2, L=0.24m, R_0=100m, z_0=0m, Ω=30RPS

The graph in the Fig. 13 is obtained as a result of calculation for the condition that it is L=0.24m and Ω=30RPS. If we put now these values in the equation (8), we obtain that K_m=20.55.

Starting from this value of K_m, the value of elevation angle β_m (which is determined by some other algorithm of drone DILC process on FMCW radar) and the value of Δ_m from the analyzed spectrogram, it is possible to calculate the value of the product

$$L_m \cdot \Omega_m = \frac{\Delta_m}{K_m \cdot \cos(\beta_m)} \tag{9}$$

Further, if Ω_m is determined from the appearance of the spectrogram part with higher frequency components, it is possible to calculate the length of blades as

$$L_m = \frac{\Delta_m}{K_m \cdot \Omega_m \cdot \cos(\beta_m)} \tag{10}$$

VI. Conclusions

In this paper we have presented the initial development of a program for calculation and presentation of drones' micro-Doppler spectrograms as well as some results of its implementation. The benefits of such program application are that it is not necessary to have a high number of different drones and to perform significant volume of recording during drones operation in order to form the base of their spectrograms. This program follows the analytical model from [29]. The initial modelling is limited to hovering drones whose rotors have equal angular rotation rate. A number of spectrograms with differently defined input parameters is presented in the paper. The method for determination of drone's flight and construction characteristics is defined on the base of presented spectrograms. The number of blades in each rotor, rotors' angular rotation rate and blades' length, which contribute to specificities of spectrograms, may be concluded on the base of spectrograms appearance.

These initial calculations and presentations are performed in Excel as other, more suitable possibilities, were not available to us. Excel allows to perform good quality presentations of calculation results, as is also demonstrated in our contribution [43]. We plan to perform future investigations in some more powerful surrounding where it would be possible to model drone flying (besides hovering). It is also necessary to model drones with higher number of rotors (hexacopters, octocopters) as well as drone swarms to further improve drones DILC by FMCW radars.

FMCW radars are not the only way to obtain spectrograms as the ones presented in this paper. The similar results may be also obtained by using pulsed radar where the returned pulse delay is the measure of Doppler shift [13]. IRITEL already has experience in the development and improvements of such radars [21], [26]-[28]. In the case of single carrier radar the measure of Doppler shift would be the change of returned signal phase which is more complicate for realization.

References

[1] G. Delauney, "Mystery drone from Ukraine war crashes in Croatia," BBC News, Balkans correspondent, https://www.bbc.com/news/world-europe-60709952.

[2] N. Razzouk, J. Blas, J. Thornhill, "Speed of Saudi Oil Recovery in Focus After Record Supply Loss," Bloomberg, 15. September 2019.,

 ISBN 978-86-7466-930-3

https://www.bloomberg.com/news/articles/2019-09-15/saudis-race-to-restore-oil-output-after-crippling-aramco-attack.
[3] N. Eriksson, "Conceptual study of a future drone detection system Countering a threat posed by a disruptive technology," Master thesis in Product Development, Chalmers University of Technology, Goethenburg, Sweden, 2018.
[4] V. Matić, V. Kosjer, A. Lebl, B. Pavić, J. Radivojević, "Methods for Drone Detection and Jamming," 10th International Conference on Information Society and Technology (ICIST), Kopaonik, March 8-11., 2020., in: Zdravković, M., Konjović, Z., Trajanović, M. (Eds.) ICIST 2020 Proceedings Vol. 1, pp.16-21, 2020.
[5] Advanced protection systems: "Ctrl+sky drone detection and neutralization system," 2017., http://apsystems.tech/wp-content/uploads/2018/01/aps_broszura_web.pdf.
[6] X. Shi, C. Yang, C. Liang, Z. Shi, and J. Chen: "Anti-Drone System with Multiple Surveillance Technologies: Architecture, Implementation, and Challenges," IEEE Communications Magazine, Vol. 56, Issue 4, April 2018., pp. 68-74., DOI: 10.1109/MCOM.2018.1700430.
[7] F. Fioranelli, O. Krasnov, Y. Cai, A. Yarovoy, J. Yun, D. Anderson, "MSG-SET-183 Specialists' Meeting – Improving the Simulations of Radar Signatures of Small Drone," STO-MP-MSG-SET-183, NATO, S&T organization, pp. 1-1 – 1-12.
[8] V. M. Milovanović, "On Fundamental Operating Principles and Range-Doppler Estimation in Monolithic Frequency-Modulated Continuous-Wave Radar Sensors," *Facta Universitatis, Series: Electronics and Energetics*, Vol. 31, No. 4, pp. 547-570, December 2018, DOI: https://doi.org/10.2298/FUEE1804547M.
[9] A. De Luca, "Forward Scatter Radar: Innovative Configurations and Studies," PhD Thesis, University of Birmingham, February 2018.
[10] C. Zhao, G. Luo, Y. Wang, C. Chen and Z. Wu, "UAV Recognition Based on Micro-Doppler Dynamic Attribute-Guided Augmentation Algorithm," *Remote Sensing*, Vol. 13, No. 6, Article 1205, pp. 1-17., March 2021., DOI: https://doi.org/10.3390/rs13061205.
[11] S. A. Musa, R. A. R.Syamsul Azmir, A. Sali, A. Ismail, N. Emleen, A. Rashid, "Micro-Doppler signature for drone detection using FSR: a theoretical and experimental validation," *The Journal of Engineering*, IET International Radar Conference (IRC2018), 17-19th October 2018., Nanjing, China, pp. 1-6.
[12] M. Passafiume, N. Rojhani, G. Collodi and A. Cidronali, "Modeling Small UAV Micro-Doppler Signature Using Milimeter-Wave FMCW Radar," *Electronics 2021*, Vol. 10, pp. 1-16., https://doi.org/10.3390/electronics10060747.
[13] S. Rahman, D. A. Robertson, "Radar micro-Doppler signatures of drones and birds at K-band and W-band," *Scientific Reports*, Vol. 2018, No. 8, pp. 1-11., November 2018., DOI: 10.1038/s41598-018-35880-9.
[14] A. Lebl, M. Mileusnić, D. Mitić, J. Radivojević, V. Matić, "Verification of Calculation Method for Drone Micro-Doppler Signature Estimation," accepted for publication in *Facta Universitatis, Series: Electronics and Energetics*, ISSN: 0353-3670.
[15] P. Jovanović, M. Mileusnić, B. Pavić, B. Mišković, "DDS based Pulse-Doppler Radar Transmitter Simulator," XIII International Scientific-Professional Symposium INFOTEH Jahorina, March 2014., Vol. 13. Ref. B-II-5, pp. 425-428.
[16] V. Marinković, B. Pavić, A. Toth, "Radar Signal Simulator for New Generation Digital Radar Receiver," INFOTEH Jahorina, Vol. 7. Ref. B-II-18, March 2008., pp. 228-231., in Serbian.
[17] B. Pavić, B. Mišković, V. Marinković-Nedelicki, M. Mileusnić,P. Petrović, "Projekat simulatora impulsnih radarskih signala," tehničko rešenje u kategoriji M85 na projektu tehnološkog razvoja TR32051 pod nazivom "Razvoj i realizacija naredne generacije sistema, uređaja i softvera na bazi softverskog radija za radio i radarske mreže," 2016.
[18] N. Remenski, B. Pavić, M. Mileusnić, P. Petrović, "Practical Realization of Digital Radar Receiver," 49. Conference ETRAN, Budva, June 2005., pp. 105-108., in Serbian.
[19] D. Dramićanin, V. Vlahović, N. Remenski, B. Pavić, P. Petrović, "FPGA Implementation of the Digital Radar Receiver," INFOTEH 2006, March 2006., Vol. 5. Ref. B-II-2, pp. 80-84., in Serbian.
[20] N. Remenski, V. Marinković-Nedelicki, V. Tadić, P. Petrović, "The Control of New Generation Digital Radar Receiver," INFOTEH 2006, March 2006., Vol. 5. Ref. B-II-10, pp. 114-118., in Serbian.
[21] V. Marinković, N. Remenski, V. Tadić, P. Petrović, "The Software for Control of Digital Radar Receiver VHF DP/P-12," 51. Conference ETRAN, Budva, Herceg Novi – Igalo, 2007., in Serbian.
[22] V. Matić, V. Marinković-Nedelicki, V. Tadić, "Comparison of digital signal processing methods for sine wave signal generation," Proceedings of SBT/IEEE International Telecommunications Symposium ITS '98, August 1998., DOI: 10.1109/ITS.1998.713134.
[23] V. Matić, V. Marinković-Nedelicki, "The waveform generator based on digital signal processing," Proceedings of the 2000 Third IEEE International Caracas Conference on Devices, Circuits and Systems 2000, pp. T56/1-T56/6, March 2000., DOI: 10.1109/ICCDCS.2000.869878.
[24] P. Petrović, "Research in Software Defined Radio and AESA Radar Technology, Serbia-Italia/Status and Perspectives of the Scientific and Technological Bilateral Cooperation," 2012., pp. 19-20.
[25] P. Jovanović, M. Mileusnić, P. Petrović, "An Approach to Analysis of AESA Based Radio systems," XII International Scientific-Professional Symposium INFOTEH Jahorina 2013, March 2013., Vol. 12., pp. 372-376.
[26] Land-based air defence radars, Serbia: VHF DR/P-12/18, in the book M. Streetly, *Jane's Radar And Electronic Warfare Systems*, IHS Global Limited, 2011.
[27] B. Pavić, V. Marinković-Nedelicki, M. Mileusnić, N. Remenski, P. Petrović, "Verifikovani modernizovani radar P-12," tehničko rešenje – novi proizvod u kategoriji M81 na projektu tehnološkog razvoja TR32051 pod nazivom "Razvoj i realizacija naredne generacije sistema, uređaja i softvera na bazi softverskog radija za radio i radarske mreže," 2013.
[28] M. Mileusnić, B. Pavić, V. Marinković-Nedelicki, P. Petrović, V. Matić, A. Lebl, "Verifikacija razvoja i realizacije nulte serije nove varijante modernizovanog osmatačko-akvizicijskog radara P-12M," tehničko rešenje u kategoriji M82 na projektu tehnološkog razvoja TR32051 pod nazivom "Razvoj i realizacija naredne generacije sistema, uređaja i softvera na bazi softverskog radija za radio i radarske mreže," 2018.
[29] V. C. Chen, "*The Micro-Doppler Effect in Radar*," Artech House, Second Edition, 2019., ISBN: 978-1-63081-546-2.
[30] C. R. Ferreiro, "Modeling and Analysis of Micro-Doppler Signatures for Radar Target Classification," Thesis for Bachelor in telecommunication Engineering, Telecommunication Engineering School, Universida de Vigo, 2017.
[31] R. W. Deters, S. Kleinke, "Static Testing of Propulsion Elements for Small Multirotor Unmanned Aerial Vehicles," AIAA AVIATION Forum, 35th AIAA Applied Aerodynamics Conference, 2017-3743, 5-9. June 2017., Denver, Colorado, pp. 1-34.
[32] Drone Tech Planet, "How a Quadcopter Works Along With Propellers and Motors," https://www.dronetechplanet.com/how-a-quadcopter-works-along-with-propellers-and-motors/.
[33] "Mavic Mini Propellers," https://store.dji.com/product/mavic-mini-propellers.
[34] "DJI Mavic 3 Low-Noise Propellers," https://store.dji.com/product/dji-mavic-3-low-noise-propellers.
[35] "DJI Propeller Set for Phantom 4 Pro/Pro+ V2.0 (2 Pack)," https://www.bhphotovideo.com/c/product/1407136-REG/dji_cp_pt_00000274_01_propellers_for_phantom_4.html/specs.
[36] "Altair 818 Hornet Propellers," https://altairaerial.com/products/aa818-plus-drone, https://www.amazon.com/Altair-818-Hornet-Propellers/dp/B07819RC9Q.
[37] 911, Rotorcraft, "Types of Drones," https://www.911security.com/learn/airspace-security/drone-fundamentals/types-of-drones-rotorcraft.
[38] M. Ahmadizadeh, "An Introduction to Short-Time Fourier Transform (STFT)," Sharif University of Technology, Department of Civil Engineering, July 2014.
[39] H. A. Gaberson, "A Comprehensive Windows Tutorial,"*Sound and Vibration*, Instrumentation Reference Issue, March 2006., pp. 14-23.
[40] C. Zhao, G. Luo, Y. Wang, C. Chen and Z. Wu, "UAV Recognition Based on Micro-Doppler Dynamic Attribute-Guided Augmentation Algorithm," *Remote Sensing*, Vol. 13, No. 6, Article 1205, pp. 1-17., March 2021., DOI: https://doi.org/10.3390/rs13061205.
[41] P. K. Rai, A. Kumar, M. Z. Ali Khan, J. Soumya, L. Reddy, "Angle and Height Estimation Technique for Aerial Vehicles using mmWave FMCW Radar," 2021 International Conference on COMmunication Systems & NETworkS (COMSNETS), 5-9. January 2021., Bangalore, India, DOI: 10.1109/COMSNETS51098.2021.9352744.
[42] P. K. Rai, H. Idsoe, R. R. Yakkati, A. Kumar, M. Z. Ali Khan, P. K. Yalavarthy, "Localization and Activity Classification of Unmanned Aerial Vehicle Using mmWave FMCW Radars," IEEE Sensors Journal, Vol. 21, No. 14, pp. 16043-16053., July 2021., DOI: 10.1109/JSEN.2021.3075909.
[43] J. Radivojević, B. Pavić, A. Lebl, M. Petrović, "Sweep Jamming with Discrete Subbands – an Advanced Strategy for Malicious Drones Missions Prevention," Scientific Technical Review, Vol. 71, No. 2, March 2022, pp. 46-52., ISSN: 1820-0206, UDK: 355.43:623.624,449.8, COSATI: 03-10, 14-04-01, DOI: 10.5973/str2102046R.